Geophys. J. Int. (2002) **148,** 329–335

Global heat flow simulation based on a kinematic model of mantle flow

Zheng-Ren Ye and Jian Wang

Institute of Geology & Geophysics, Chinese Academy of Sciences, Beijing 100101, *China. E-mail: zrye@mail.c-geos.ac.cn*

Accepted 2001 September 24. Received 2001 June 20; in original form 2000 August 18

SUMMARY

The global heat flow is the surface representation of thermal processes within the earth's mantle. The long-wavelength pattern of observed heat flow closely resembles the plate tectonics and its most prominent feature is higher values along ocean ridge systems. Theoretically, to determine the thermal state of the Earth's mantle, the heat transfer problem and the mantle convection problem have to be solved simultaneously since they are coupled with each other. However, the development of global seismic tomography provides us with a possibility that, at least under certain assumptions, these problems can be decoupled from each other and solved separately. This allows us to calculate mantle flow velocities first based on the internal loading theory and then use the velocity field as the input to solve the thermal problem. In addition to the internal density anomalies, surface plate movements also excite mantle circulations and, under certain circumstance, they may dominate the structure of the mantle flow.

In this study, using a kinematic model of mantle convection and heat transfer, we investigated the underlying processes that generated the observed global heat flow. Buoyancy from the density anomalies and the coupling from the overlying plates are treated as the mantle flow driving force. Both advection and conduction heat transfers are included in the energy equation. Results show that calculated depth derivatives of the near surface temperature are closely correlated to the observed surface heat flow pattern. Higher heat flow values around mid-ocean ridge systems can be reproduced very well. The predicted average temperature as a function of depth reveals that there are two thermal boundary layers, one is close to the surface and another is close to the core–mantle boundary. The rest of the mantle is nearly isothermal. Although, in most of the mantle, advection dominates the heat transfer, the conductive heat transfer is still locally important in the boundary layers and plays an important role for the surface heat flow pattern. The existence of surface plates is responsible for the long wavelength surface heat flow pattern.

Key words: density anomaly, heat flow, mantle flow, plate motion, tomography.

1 INTRODUCTION

The global heat flow is of significance because it provides an important constraint that any dynamic model of the Earth must accommodate. With increasing observations, we now have a relatively accurate understanding on its regional variations. One of the most prominent features of the global heat flow is the higher value along the ocean ridge systems that closely resemble the global plate tectonics (Pollack *et al.* 1993; Sclater *et al.* 1980; Chapman & Pollack 1975; Deelinger 1992). Variations in heat flow (as well as sea-floor depth) versus the distance away from mid-ocean ridges can be explained within the framework of plate tectonics. Both the plate-moving model and the half-space cooling model (Parson & Sclater 1977; Davis & Lister 1974) well explain the relationship between the variation in heat flow and the ocean floor age. These theories predicted that heat flows decrease with age$^{-1/2}$ when away from ridge crests (Stein & Stein 1992). However, all these works were based on 1-D analyses.

Recently, Pari & Peltier (1998) gave an explanation of the global heat flow pattern in terms of tomography-based mantle flow, in which they assumed that the heat flow is linearly related to the radial component of flow velocity in the uppermost mantle.

In this paper, we are aiming to model the global surface heat flow. Instead of using a 1-D heat transfer model or assuming a simple relationship between the mantle flow velocity and the heat flow, we try to simulate the global heat flow distribution by formally solving the energy equation and calculate the temperature field. Theoretically, the convection pattern and temperature field of the earth's mantle should be determined by simultaneously solving the coupled momentum equation and energy equation. However, the new

results from global seismic tomography provide us with the information on 3-D seismic velocity anomalies in the mantle. Based on this information and under certain approximations, mantle flow and temperature field can be solved separately. Following this approach, the moment equation is solved first. Density anomalies derived from seismic tomography are treated as sources of the buoyancy exciting the mantle flow. Mantle flow velocities can then be obtained based on the internal loading theories (Hager 1984; Richards & Hager 1984; Ricard & Vigny 1989; Forte & Peltier 1991; Ye *et al.* 1996). In addition to the internal density anomalies, surface plate movements can also drive the mantle circulation. Sometimes, they will even dominate part of the flow structure in the mantle (Zhong *et al.* 2000). After mantle flow velocities are obtained, they can be used in the energy equation for solving the global temperature distribution and surface heat flow (Pari & Peltier 1998; Ye & An 1999). All these processes, mantle flow, heat transfer and surface heat flow, are examined in a 3-D spherical geometry frame.

2 3-D MODEL OF MANTLE TEMPERATURE

The mantle is assumed to have an infinite Prandtl number Pr ($\mathrm{Pr} = \nu/k$, where ν is the kinemitic viscosity and k is the thermal diffusivity); behaving as an incompressible Newtonian fluid; and having a radial symmetric shell viscosity structure. Because of the infinite Pr number, the inertial term in the momentum equation is negligible. Equations governing the mantle flow reduce to

$$\nabla \cdot \mathbf{v} = 0 \tag{1a}$$

$$\nabla \cdot \boldsymbol{T} + \delta\rho g = 0 \tag{1b}$$

$$\boldsymbol{T} = -p + 2\mu(r)\varepsilon \tag{1c}$$

where $\mathbf{v}$ is the velocity, $\boldsymbol{T}$ is the stress tensor, $\delta\rho$ is the density anomaly, g is the gravitational acceleration, p is the pressure, μ is the viscosity and ε the strain tensor. Several approaches have been proposed to solve these equations within a spherical frame (Backus 1967; Hager & O'connell 1978; Richards & Hager 1984; Forte & Peltier 1987). The basic technique is to convert partial differential equations into a set of radial-dependent first-order ordinary differential equations by introducing velocity-stress vectors and spherical harmonic expansions. Then solve the two-point boundary value problems of resulted ODEs. Here, we just write down these ODEs as our working equations:

$$\frac{d\mathbf{X}_1^{\mathbf{lm}}}{dr} = \mathbf{A}_\mathbf{l}\mathbf{X}_1^{\mathbf{lm}} + \mathbf{D}^{\mathbf{lm}} \tag{2a}$$

$$\frac{d\mathbf{X}_2^{\mathbf{lm}}}{dr} = \mathbf{B}_\mathbf{l}\mathbf{X}_2^{\mathbf{lm}} \tag{2b}$$

where $\mathbf{X}_1^{\mathbf{lm}} = (\mathrm{U}^{\mathrm{lm}}, \mathrm{V}^{\mathrm{lm}}, \mathrm{P}^{\mathrm{lm}}, \mathrm{Q}^{\mathrm{lm}})^{\mathrm{T}}$ and $\mathbf{X}_2^{\mathbf{lm}} = (\mathrm{W}^{\mathrm{lm}}, \mathrm{R}^{\mathrm{lm}})^{\mathrm{T}}$ are velocity-stress vectors, **l** and **m** are degree and order numbers of poloidal and toroidal components, respectively, A_l and B_l are 4×4 and 2×2 matrixes depending on the viscosity profile. The inhomogeneous term $\mathbf{D}^{\mathbf{lm}}$ is the mantle flow driving force resulting from internal density anomalies. Before we can solve eqs (2a) and (2b), necessary boundary conditions are required. At the core–mantle boundary, we use the condition that materials are free to slip because of the very low viscosity in the outer core. At the surface of the Earth, horizontal velocities derived from observed angular velocities of plate motions, i.e., the AM2 model from Minster & Jordon (1978), are applied. Since these plates are treated as active boundary conditions, they will also excite mantle flows.

After mantle flow velocities excited by density anomalies and plate movements were obtained, we want to estimate their influence on the temperature distribution. Theoretically, whether or not the material flux significantly disturbs the initial temperature distribution depends on the non-dimensional number Pe (Tritton 1977). The Peclet number Pe is defined as $\mathrm{Pe} = UL/k$, where U and L are scales of the velocity and the length of the system and k is the thermal diffusivity. The Peclet number can be interpreted as a measure of the relative importance of the heat advection and conduction. For the mantle dynamic system, the thermal diffusivity k is in the order of 10^{-6} m^2 s^{-1}. Taking the typical plate motion velocity and the depth of the core–mantle boundary as velocity and length scales, we have an estimation of several thousands for the Peclet number, a value large enough to significantly influence the initial conductive temperature field in the mantle and hence the heat flow distribution pattern at the surface of the Earth. The non-dimensional energy equation describing temperature field is

$$\frac{\partial\theta}{\partial t} + \mathbf{v} \cdot \nabla(\theta + \theta_c) = \nabla^2\theta. \tag{3}$$

Here the first term on the left hand side of eq. (3) is the time variation of the temperature, the second term is advection heat transfer and the right hand side is the conductive heat transfer. Due to a high Peclet number, advection heat transfer is dominant in most of the mantle. However, the conductive term may still be locally important. For example, in boundary layers near the surface and core–mantle boundary, velocities are nearly perpendicular to temperature gradients and the advection heat transfer is inefficient. These regions are particularly important to problems such as surface heat flows and the thermal history of cooling oceanic plates, etc. For this reason, we keep both advection and conduction terms, together with the time variation term, in our energy equation.

To solve the energy equation, the temperature is divided into two parts. θ_c is the temperature distribution under a purely conductive state, satisfying the 1-D homogeneous Laplace equation and can be obtained under the boundary conditions of $\theta_c = 0$ at the Earth's surface and $\theta_c = 1$ at the core–mantle boundary. The process yields $\theta_c(r) = r_c r_s/r - r_c$, where the modifiers c and s denote non-dimensional radius at the core–mantle boundary and the surface, respectively. θ is the temperature deviation from the conductive state. The non-dimensional scales used for length, time, velocity and temperature are d, d^2/k, k/d and ΔT, where d is the depth of the core–mantle boundary, k is the thermal diffusivity and ΔT is the temperature difference between the surface and the core–mantle boundary. The non-dimensional boundary conditions for θ are $\theta = 0$ at both the surface and the core–mantle boundary.

We use the spherical harmonic expansion and the Galerkin method (Zebit *et al.* 1980) to find out the solution of eq. (3) under the boundary conditions mentioned above. The longitudinal and latitudinal dependents of the temperature field are expanded using spherical harmonics and its radial-dependent is expanded using a set of trigonometric functions, which automatically satisfy the boundary conditions.

$$\theta(t, r, \lambda, \phi) = \sum_{l=0}^{\infty}\sum_{m=-l}^{l}\sum_{j=1}^{\infty}\Theta_{jlm}(t)Y_{lm}(\lambda, \phi)C_j \tag{4}$$

where $C_j = \sqrt{2}\sin[j\pi(r - r_c)]$. Substituting (4) into the temperature eq. (3), multiplying it by $C_k = \sqrt{2}\sin[k\pi(r - r_c)]$ and integrating from r_c to r_s, the procedure eventually leads to a set of initial value problems for expansion coefficients $\Theta_{jlm}(t)$

$$\frac{d\Theta_{klm}}{dt} = \sum_{j=1}^{\infty} \alpha_{ljk}\Theta_{jlm} - \sum_{j=1}^{\infty}\sum_{l_2=0}^{\infty}\sum_{m_2=-l_2}^{l_2} F(k,l,m,j,l_2,m_2)\Theta_{jl_2m_2} + \beta_{klm}$$
$$k = 1,\ldots,\infty; l = 0,\ldots,\infty; m = -l,\ldots,l \quad (5)$$

where

$$\alpha_{ljk} = \int_{r_c}^{r_s} C_j D_l C_k \, dr, \qquad D_l = \frac{d}{dr^2} + \frac{2}{r}\frac{d}{dr} - \frac{l(l+1)}{r^2}$$

$$\beta_{klm} = \int_{r_c}^{r_s} \left(\frac{r_c r_s}{r_s - r_c}\right) \frac{\mathrm{U}^{\mathrm{lm}}(r)}{r^2} C_k \, dr$$

$$F(k,l,m,j,l_2,m_2) = \frac{1}{4\pi}\sum_{l_1=0}^{\infty}\sum_{m_1=-l_1}^{l_1}\left[p_1\int_{r_c}^{r_s}\mathrm{U}^{\mathrm{l_1m_1}}(r)C_k\frac{dC_j}{dr}\,dr + p_2\int_{r_c}^{r_s}\mathrm{V}^{\mathrm{l_1m_1}}(r)\frac{C_jC_k}{r}\,dr + p_3\int_{r_c}^{r_s}\mathrm{W}^{\mathrm{l_1m_1}}(\mathrm{r})\frac{\mathrm{C_jC_k}}{\mathrm{r}}\,dr\right]$$

$$p_1 = \iint_{\Omega} Y_{l_1m_1} Y_{l_2m_2} Y^*_{lm}\, d\Omega$$

$$p_2 = \iint_{\Omega} \left(Y^{\lambda}_{l_1} Y^{\lambda}_{l_2} + Y^{\phi}_{l_1} Y^{\phi}_{l_2}\right) Y^*_{lm}\, d\Omega$$

$$p_3 = \iint_{\Omega} \left(Y^{\phi}_{l_1} Y^{\lambda}_{l_2} - Y^{\lambda}_{l_2} Y^{\phi}_{l_2}\right) Y^*_{lm}\, d\Omega$$

where Y_{lm} is fully-normalized surface harmonics of degree l and order m.

$$Y^{\lambda}_l \equiv \frac{\partial Y_{lm}}{\partial \lambda}, \qquad Y^{\varphi}_l \equiv \frac{1}{\sin\lambda}\frac{\partial Y_{lm}}{\partial \varphi} \quad (6)$$

U^{lm}, V^{lm}, W^{lm} are components in velocity-stress vectors, respectively. Noting that in eq. (5) modes Θ_{jlm} are coupled with each other, which results from the contribution of the advective heat transport. Since the above summations go to infinity, we have no obvious way to solve these equations. However, if we truncate the summations up to l_{max} and j_{max}, we will have a finite number of linear ordinary differential equations that can be numerically integrated with arbitrary values of Θ_{jlm}. For different initial values, numerical tests reveal that a steady state can be reached after a relatively short time interval.

3 RESULTS

There are two factors affecting the mantle flow structure. One is the depth dependence of the mantle viscosity; another is the proportional factor between density anomaly and seismic velocity anomaly in the mantle. To investigate the sensitivity of mantle viscosity, four viscosity models are used in our numerical calculations. These viscosity models are shown in Fig. 1(a). Model 1 has a constant viscosity of 10^{21} Pa s throughout the mantle. Model 2, which is adopted from Richards & Hager (1984), has a high viscosity lower mantle that is 30 times higher than that of the upper mantle. Model 3 differs from Model 2 in that there is a lower viscosity layer (0.032×10^{21} Pa s) between depths 100 and 400 km. Model 4 is same as model 3 except that the viscosity in the uppermost 100 km is 10^{22} Pa s.

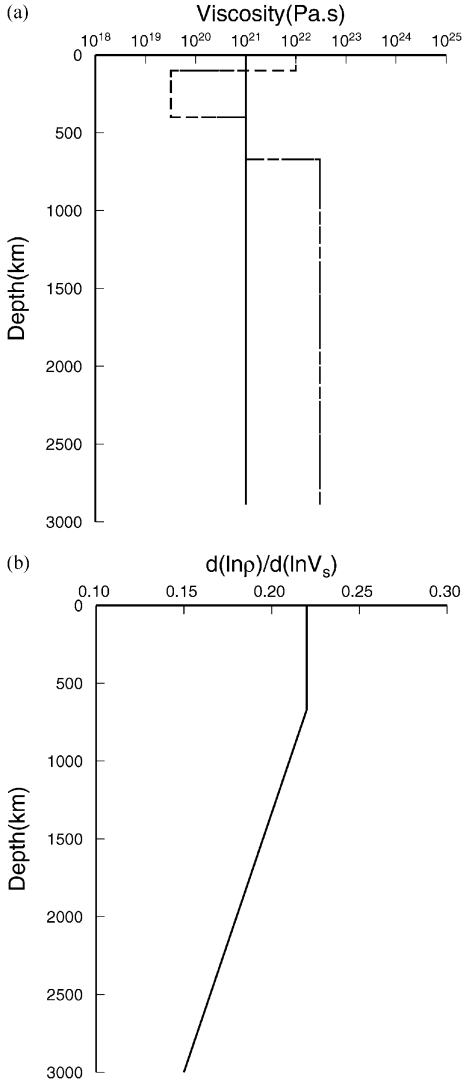

Figure 1. (a) Viscosity models. Solid line denotes Model 1 that is a constant viscosity model. Dashed line is Model 2. Dot line is for Model 3 and short dashed line is for Model 4. (b) The depth dependence of the proportional factor between density and seismic S-wave velocity ($d\ln\rho/d\ln v_s$), used in the study. After Pari & Peltier (1995).

The relationship between density anomalies and seismic velocity anomalies shows complexity since in different regions, e.g. deep continental roots, subducted lithosphere and the D″ layer, chemical heterogeneities may play different roles. Some results were derived in recent years (Ricard *et al.* 1989; Forte *et al.* 1994; Karoto 1993; Pari & Peltier 1995). In this work, we use a depth dependent proportional factor to link the density and the S-wave velocity ($d\ln\rho/d\ln v_s$). This factor is similar to that suggested by Pari & Peltier (1995). In the upper mantle the factor is 0.22. It decreases linearly with depth in the lower mantle and reaches to 0.15 at the core–mantle boundary. Fig. 1(b) gives the depth dependence of this factor. During the last decade, several new global seismic tomographic models have been published and they gave fairly consistent results for lower degree velocity anomalies of the Earth's mantle. The SH12WM13 model by Su *et al.* (1994) is chosen as the input data in this work.

Based on a large number of heat flow data, Pollack *et al.* (1993) worked out a spherical harmonic representation of the global heat

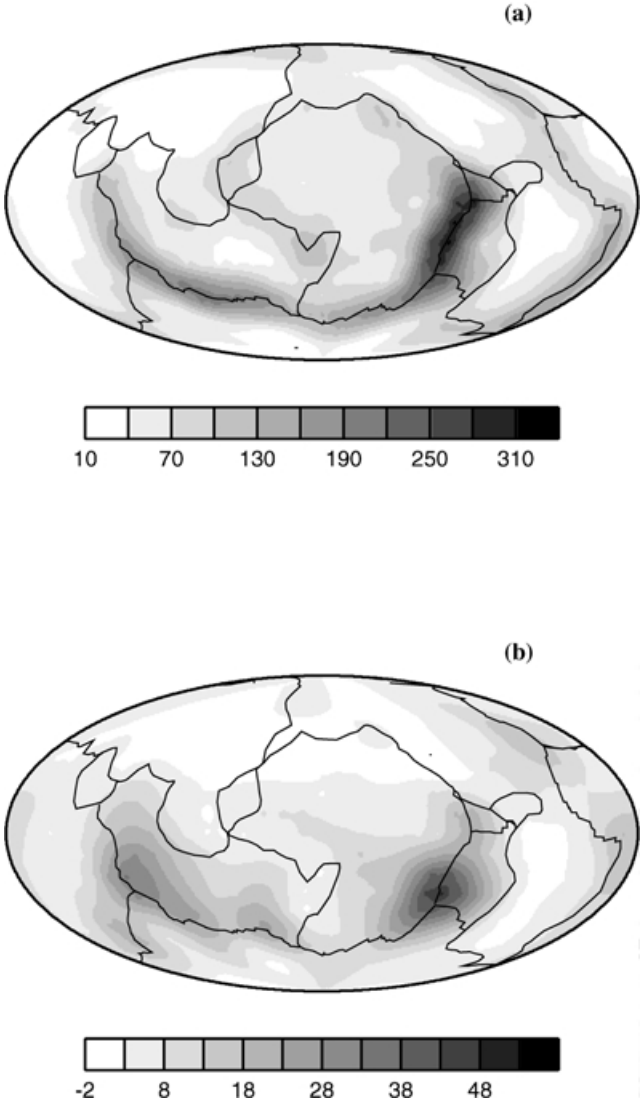

Figure 2. Comparison between observed global heat flow and predicted depth derivatives of near surface non-dimensional temperature. Both of them are summed up to degree and order 12. (a) is the observed global heat flow in mw m^{-2} which has been modified by the stripping of continental crustal radioactivity according to Pari & Peltier (1998). (b) is predicted depth derivatives of near surface non-dimensional temperature for viscosity Model 2. Both density anomaly-driven and plate-driven mantle flows are considered.

flow. In their model, contributions from the crustal radioactivity and the associated fraction of primarily continental heat flux were not taken into account. Pari & Peltier (1998) introduced a 'continental function' to correct the original observations. A 0 to 12 the degree representation of the modified heat flow is presented in Fig. 2(a) on which plate boundaries are also superimposed. The higher heat flow values around the mid-ocean ridge system, especially near the East Pacific Rise and the East Indian Ridge are clearly shown in this figure.

The depth derivatives of the near surface non-dimensional temperature (i.e., the radial components of the near surface temperature gradients), which are proportional to the surface heat flows, are simulated for four different viscosity models using the method provided in Section 2. Depth derivatives of near surface temperatures (summed up to degree 12) for viscosity Model 2 are shown in

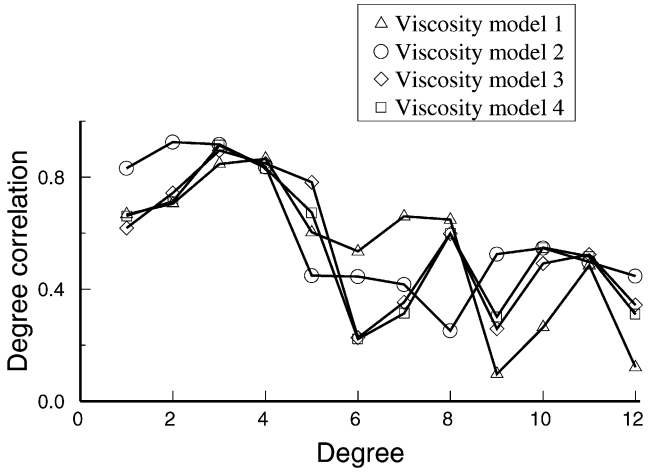

Figure 3. Degree correlations between the observed surface heat flow and predicted near surface temperature gradients for four viscosity models.

Fig. 2(b). From the figure it can be seen that predicted heat flows match the observations (Fig. 2a) very well. The areas around the East Pacific Rise and the Indian Ridge show much higher temperature gradients than the rest of the world. The relatively higher values of the heat flow around the Mid-Atlantic Ridge are also reflected in the simulation. The locations of the higher temperature gradients calculated are migrated slightly from observed maximum heat flows in three oceanic ridges (Figs 2a and b). There are also some mismatches in subduction zones in West Pacific Ocean. These errors may result from the fact that the current calculation is based on a kinematic model and the loading systems (both density anomalies and plate motions) are time invariant.

Degree correlations between calculated depth derivatives of near surface temperature and observed heat flows for four viscosity models are shown in Fig. 3. The degree correlation $\gamma(l)$ for functions $F(\lambda, \varphi)$ and $G(\lambda, \varphi)$ on a spherical surface is defined as

$$\gamma(l) = \frac{\sum_{m=-l}^{l} F_{lm} G_{lm}^{*}}{\left[\left(\sum_{m=-l}^{l} F_{lm} F_{lm}^{*}\right)\left(\sum_{m=-l}^{l} G_{lm} G_{lm}^{*}\right)\right]} \tag{7}$$

where, F_{lm} and G_{lm} are spherical harmonic coefficients, l and m are degree and order numbers of F and G. By examining Fig. 3 we can see that correlations between the observed heat flow and the predicted surface temperature gradients for degrees 1–5 and for all four viscosity models are good. Fig. 4 shows variances of observed heat flows and calculated surface temperature gradients versus degree numbers for viscosity model 2. These variances are normalized according to the RMS value of the degree 1 variance that has been set to unity. Observations and predictions show similar decaying slopes with the increasing of degree numbers.

Included in Fig. 5 is the spherically averaged non-dimensional temperature (total temperature $\theta + \theta_c$) versus depth for viscosity Model 2. The adiabatic temperature variation is not included. Thermal boundary layers with rapid temperature variations near the Earth's surface and the core–mantle boundary are clearly seen. Within about 150 km of the top of the mantle, the mean temperature quickly rises from its surface value to an isothermal state and keeps that until it reaches the bottom of the lower mantle where, again, it increases rapidly to the core–mantle boundary temperature. These features are consistent with our knowledge of the thermal structures within the lithosphere and the D″ layer. Fig. 6 shows the average depth derivative of temperature versus the depth. The temperature

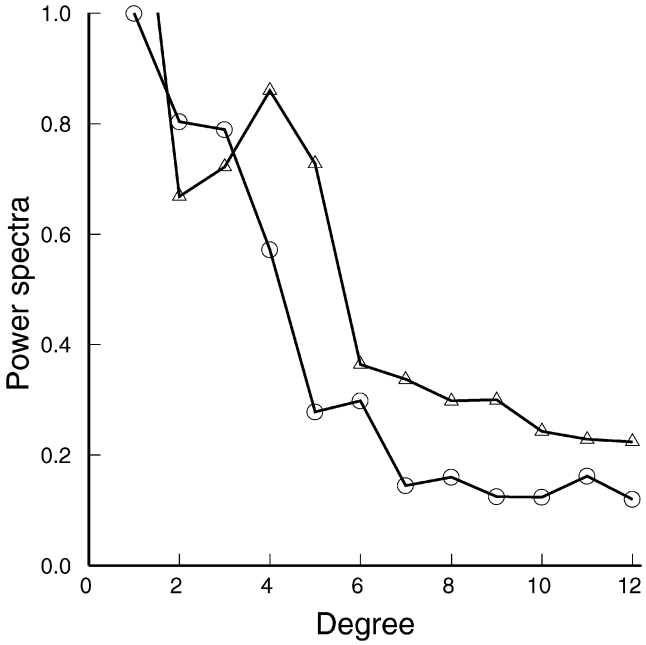

Figure 4. Degree variances for the observed heat flow (△) and the predicted surface temperature gradient (○). Curves have been normalized to have a unity RMS amplitude at degree 1. Both plate-motion and density-anomaly driven mechanisms are considered.

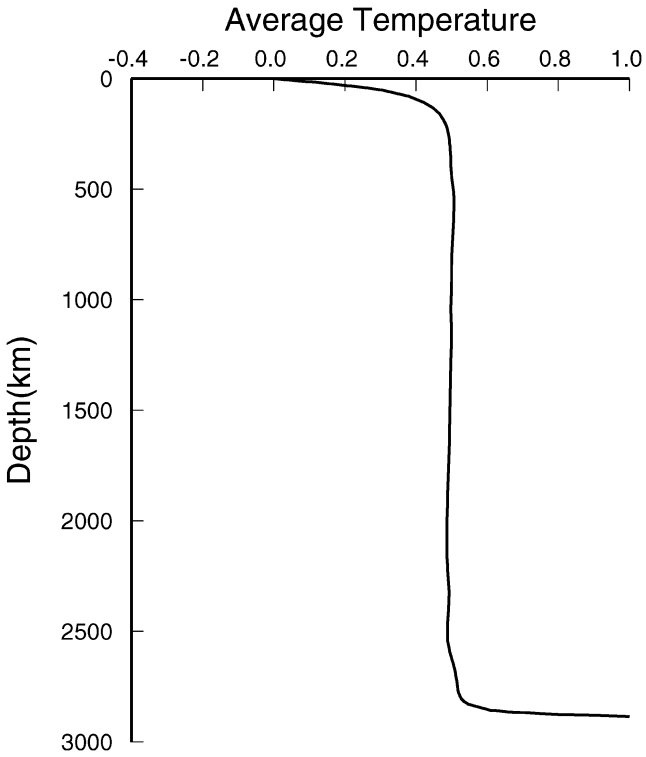

Figure 5. Spherically averaged non-dimensional temperature as a function of depth.

gradient reaches its maximum value at the Earth's surface and the core–mantle boundary, and vanishes in the near isothermal mantle.

Figs 5 and 6 suggest that the initial conductive state of the temperature field has been changed significantly due to the convective heat transfer in the mantle. Both internal density anomalies and surface

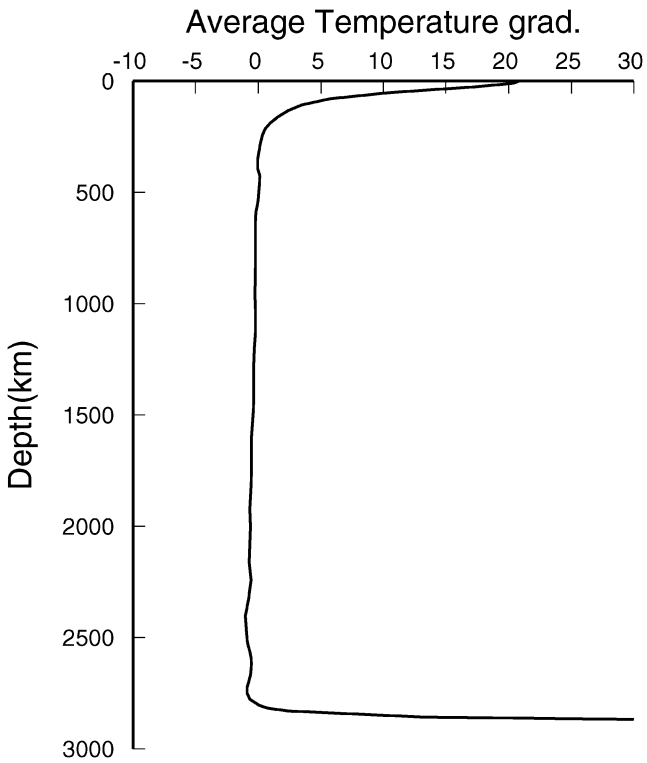

Figure 6. Spherically averaged depth derivative of the non-dimensional temperature as a function of depth.

plate motions excite mantle flows. To examine the relative importance of these factors on heat transportation, we separate these two cases. In the first case, the mantle flow is solely generated by the (tomography based) internal density anomalies, and in the second case the mantle flow is excited by surface plate motions only. The power spectrum variations of the surface temperature gradients as functions of harmonic degrees for two cases are shown in Fig. 7. It is clear that for higher degree (6–12) components, both internal density anomalies and surface plate movements have nearly the same influence. On the contrary, for lower degree (1–5) components, the power from the plate-driven mantle flow is much larger than that due to internal density anomalies. Bearing in mind that near-surface depth derivatives of the temperature (or equivalently radial components of temperature gradient) are proportional to the surface heat flow, the result suggests plate motions probably play a more important role in generating observed very long wavelength heat flow patterns.

4 CONCLUSIONS AND DISCUSSION

Global heat flow is an important observation associated with the thermal and dynamical processes in the earth's mantle. In this study, we investigated the origin of the global heat flow pattern based on a kinematic mantle flow model. The mantle flow is driven by internal density anomalies and surface plate motions. Results show that the observed global heat flow can be explained well using such a model. Various characteristics including the higher heat flow values around mid-ocean ridge systems can be properly recovered. The predicted and observed surface heat flows show similar power decays versus spherical harmonic degrees. In addition to the lateral characteristics, the radial variation of the mantle temperature field is also an important indicator. The laterally averaged temperature versus depth

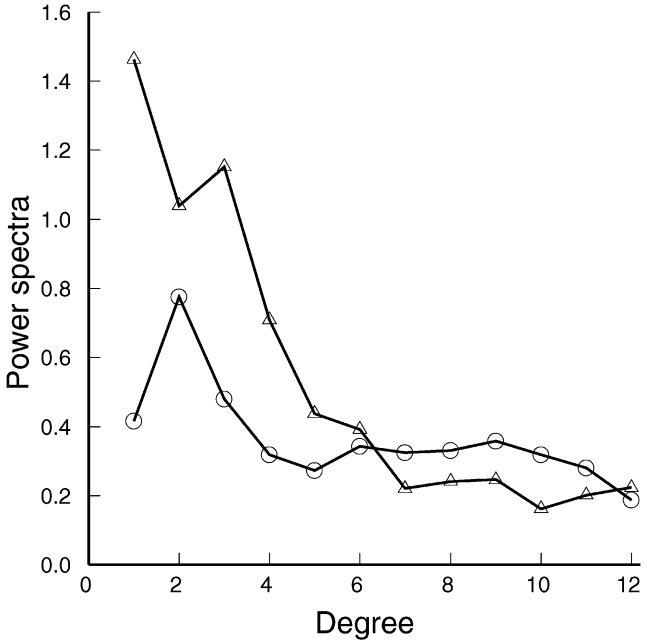

Figure 7. Power spectrum variations of the surface temperature gradients as functions of harmonic degrees for two cases: the mantle flow is solely generated by internal density anomalies (○); and excited by surface plate motions (△).

reveals a near isothermal mantle and two thermal boundary layers near the surface and the core–mantle boundary for all four viscosity models. Within the topmost 150 km, roughly the thickness of the lithosphere, the temperature raises rapidly. These features are consistent with our knowledge of the mantle thermal state.

It was suggested that plate motions might strongly affect the flow pattern due to their coupling with the underlying mantle (Hager & O'connell 1981; Davies 1988). This primarily results from high strength overlying plates that compress small-scale circulations and enhance large-scale circulations. Consequently, the mantle thermal structure will be dominated by plate-scale modes (Davies & Richards 1992). Results from our global heat flow simulation supported these points. Compared with the density anomaly-driven mantle flow, the plate-driven mantle flow dominates the calculated surface heat flow pattern especially for very long wavelength components. It is interesting that calculated surface temperature gradients are relatively insensitive to the radial viscosity structures (Fig. 3). Pari & Peltier (1995) examined the effect of a mantle viscosity structure on the heat flow profile generated by internal density anomalies and obtained a similar result.

Correlation between the observed heat flow and calculated depth derivatives of near surface temperature is good for lower harmonic degrees ($\leq$6) and becomes poor with increasing degree numbers for all four viscosity models used in the study. One possible reason is that the numerical method used to solve eq. (3) is not accurate enough to distinguish viscosity Models 3 and 4 from Model 2. The proportional factor between seismic velocity and density anomaly is still an open question. Results from different authors show large scatters depending on data and approaches used (Hager & Richards 1989; Forte & Woodward 1997). In this study we did not examine its effect on the heat transfer. However, it is expected its impact on the surface heat flow will be small since the contribution from density anomaly-driving flow is only a small fraction compared to that due to plate-driven flow (Ye & Hager 2001).

Our work is based on a whole mantle flow model and a radial symmetric viscosity structure. Layered mantle flow and lateral variations of the viscosity as well as their effects on the mantle thermal structure will be left for the future work. In our model we did not consider the internal heat source in the mantle. The main reason is that at present we do not have a realistic description of mantle heat source. The contribution from the crustal radioactivity and the associated continental heat flux has been corrected roughly by introducing a 'continental function' (Pari & Peltier 1998). It is necessary to point out that our model is a kinematic rather than a dynamic model. The velocity and temperature fields in the mantle, which are coupled with each other, were solved separately. The plate motions were imposed as a surface load which actually are part of the convection. Han & Gurnis (1999) conducted extensive numerical tests of both dynamic and kinematic models. Their results suggested that, with properly chosen parameters, a kinematic model could reasonably recover many useful features of a fully dynamic model. In the future, numerical calculations of 3-D convection with variable viscosity (Christensen & Hager 1991; Zhang & Yuen 1995; Zhong *et al.* 2000) will undoubtedly deepen our understanding of the thermal structure and plate-like surface motion.

ACKNOWLEDGMENTS

We would like to thank G. Pari for providing us the modified harmonic coefficients of global heat flow. The authors thank reviewers for thoughtful reviews leading to an improved paper. We wish to thank Xiao-bi Xie for his great help to refine the manuscript. The work was supported by the National Science Foundation of China (No. 49974022) and Chinese Academy of Sciences (No. k2cx2-112).

REFERENCES

Backus, G.E., 1967. Converting vector and tensor equations to scalar equations in spherical coordinates, *Geophys. J. R. astr. Soc.,* **13,** 71–101.

Chapman, D.S. & Pollack, H.N., 1975. Global heat flow: A new look, *Earth planet. Sci. Lett.,* **28,** 23–32.

Christensen, U. & Hager, B.H., 1991. 3-D convection with variable viscosity, *Geophys. J. Int.,* **104,** 213–226.

Davis, E.E. & Lister, C.R.B., 1974. Fundamentals of ridge crest topography, *Earth planet. Sci. Lett.,* **21,** 405–413.

Davies, G.F., 1988. Role of the lithosphere in mantle convection, *J. geophys. Res.,* **93,** 10 451–10 466.

Davies, G.F. & Richards, M.A., 1992. Mantle convection, *J. Geol.,* **100,** 151–206.

Deelinger, R.J., 1992. A revised estimate for the temperature structure of the oceanic lithosphere, *J. geophys. Res.,* **97,** 7219–7222.

Forte, A.M. & Peltier, W.R., 1987. Plate tectonics and aspherical earth structure: the importance of poloidal—toroidal coupling, *J. geophys. Res.,* **92,** 3645–3679.

Forte, A.M. & Peltier, W.R., 1991. Voscous flow models of global geophysical observables, 1, Fowward problem, *J. geophys. Res.,* **96,** 20 131–20 159.

Forte, A.M., Woodward, R.L. & Dziewonski, A.M., 1994. Joint inversions of seismic and geodynamic data for models of three-dimensional mantle heterogeneity, *J. geophys. Res.,* **99,** 21 857–21 877.

Forte, A.M. & Woodward, R.L., 1997. Seismic-geodynamic constraints on three-dimensional structure, vertical flow, and heat transfer in the mantle, *J. geophys. Res.,* **102,** 17 981–17 994.

Hager, B.H. & O'connell, R.J., 1978. Subduction zone dip angles and flow driven by plate motion, *Tectonophysics,* **50,** 111–133.

Hager, B.H. & O'connell, R.J., 1981. A simple global model of plate dynamics and mantle convection, *J. geophys. Res.,* **86,** 4843–4867.

Hager, B.H., 1984. Subducted slabs and the geoid: Constraints on mantle rheilogy and flow, *J. geophys. Res.,* **89,** 6003–6015.

Hager, B.H. & Richards, M.A., 1989. Long-wavelength variation in Earth's geoid: Physical models and dynamical implications, *Phil. Trans. R. Soc. Lond.,* A., **328,** 309–327.

Han, L. & Gurnis, M., 1999. How valid are dynamic models of subduction and convection when plante motions are prescribed, *Phys. Earth planet. Int.,* **110,** 235–246.

Karoto, S.-I., 1993. Importance of anelasticity in the interpretation of seismic tomography, *Geophys. Res. Lett.,* **20,** 1623–1626.

Minster, J.B. & Jordon, T.H., 1978. Present-day plate motions, *J. geophys. Res.,* **83,** 5331–5354.

Pari, G. & Peltier, W.R., 1995. The heat flow constraint on mantle tomography-based convection models: towards a geodynamically self-consistent inference of mantle viscosity, *J. geophys. Res.,* **100,** 12 731–12 751.

Pari, G. & Peltier, W.R., 1998. Global surface heat flux anomalies from seismic tomography-based models of mantle flow: implications for mantle convection, *J. geophys. Res.,* **103,** 23 743–23 780.

Parson, B. & Sclater, J.G., 1977. An analysis of the variation of ocean floor bathymetry and heat flow with age, *J. geophys. Res.,* **82,** 803–827.

Pollack, H.N., Hurter, S.J. & Jonson, J.R., 1993. Heat flow from the Earth's interior: analysis of the global data set, *Rev. Geophys.,* **31,** 267–280.

Ricard, Y. & Vigny, C., 1989. Mantle dynamics with induced platetectonics, *J. geophys. Res.,* **94,** 17 543–17 559.

Ricard, Y., Vigny, C. & Froidevaux, C., 1989. Mantle heterogeneities, geoid and plate motion: A monte Carlo inversion, *J. geophys. Res.,* **94,** 13 739–13 754.

Richards, M.A. & Hager, B.H., 1984. Geoid anomalies in a dynamic earth, *J. geophys. Res.,* **89,** 5987–6002.

Sclater, J.G., Jaupart, C. & Galson, D., 1980. The heat flow through oceanic and continental crust and the heat loss of the *Earth. Rev. Geophys.,* **18,** 269–311.

Stein, C. & Stein, S., 1992. A model for the global variation in oceanic depth and heat flow with lithosphere are, *Nature,* **359,** 123–129.

Su, W.-J., Woodward, R.L. & Dziewonski, A.M., 1994. Degree 12 model of shear velocity heterogeneity in the mantle, *J. geophys. Res.,* **99,** 6945–6980.

Tritton, D.J., 1977. Physical Fluid Dynamics, 131–132, Van Nostrand Reinhold Company, New York.

Ye, Z.-R., Zhang, X.-W. & Teng, C.-K., 1996. Mantle flow with existence of plates and generation of the toroidal field, *PAGEOPH,* **146,** 573–587.

Ye, Z.-R. & An, Z.-W., 1999. Role of plate-driven mantle flow in distribution of the globale heat flow, *Science in China (Series D),* **42,** 416–422.

Ye, Z.-R. & Hager, B.H., 2001. The generation and distribution of global heat flow, *Chinese J. Geophys.,* **44,** 171–179.

Zebit, A., Schburt, G. & Straus, J.M., 1980. Infinite Prandtl number thermal convection in a spherical shell, *Fluid Mech.,* **97,** 257–277.

Zhang, S. & Yuen, D.A., 1995. The influences of lower mantle viscosity straification on 3-D spherical-shell mantle convection, *Earth planet. Sci. Lett.,* **132,** 157–166.

Zhong, S., Zuber, M.T., Moresi, L. & Gurnis, M., 2000. Role of temperature-dependent viscosity and surface plates in spherical shell models of mantle convection, *J. geophys. Res.,* **105,** 11 063–11 082.